Journal of
Marine Science and Engineering

MDPI

Article

Null Broadening Beamforming for Passive Sonar Based on Weighted Similarity Vector

Yuhao Wang and Zhenkai Zhang *

Ocean College, Jiangsu University of Science and Technology, Zhenjiang 212003, China; 211110304107@stu.just.edu.cn
* Correspondence: zhangzhenkai@just.edu.cn; Tel.: +86-138-5298-7957

Abstract: Beamforming technology is very important for passive sonar to detect targets. However, the performance of a beamformer is seriously degraded in practical applications due to the complex and changeable underwater environment. In this paper, a null broadening algorithm for passive sonar based on a weighted similarity vector is proposed for underwater fast-moving strong interference signals. First, the covariance matrix was reconstructed through the correlation between the steering vector and the subspace eigenvector, which was used to calculate the similarity vector. Then, the maximum power in the interference angle sector was used as the virtual interference source power to broaden the null in the angle sector. Next, the difference between the optimal weight vector and the similar vector was minimized, the interference-plus-noise power constraints and norm constraints were added, and the equation was written as a quadratic constrained quadratic programming (QCQP) problem, which was converted into a convex optimization problem by using the semidefinite relaxation technique. Finally, the optimal solution was calculated by using eigen decomposition. The simulation results show that the algorithm can guarantee deep nulling and effectively suppress sidelobe height under various error conditions, which shows that the proposed algorithm has a good suppression effect and strong robustness for fast strong interference.

Keywords: passive sonar; null broadening; robust adaptive beamforming; weighted similarity vector; virtual interference source

Citation: Wang, Y.; Zhang, Z. Null Broadening Beamforming for Passive Sonar Based on Weighted Similarity Vector. *J. Mar. Sci. Eng.* **2023**, *11*, 1858. https://doi.org/10.3390/jmse11101858

Academic Editor: Rafael Morales

Received: 20 August 2023
Revised: 10 September 2023
Accepted: 20 September 2023
Published: 25 September 2023

1. Introduction

The detection performance of an underwater target is very important for passive sonar. In the actual underwater weak target detection task, strong interference has a certain impact on the detection results. Therefore, beamforming technology plays an important role in this field. Capon beamforming technology is often used in passive sonar arrays to improve the detection performance of weak target signals and suppress interference [1]. However, the performance of a Capon beamformer is seriously degraded in practical applications due to the influence of array element amplitude and phase errors, array element position floating, and other problems [2]. Aiming at the problems arising from the above practical application, many robust adaptive beamforming algorithms have been proposed by scholars, such as loading algorithms [3], weight norm constraint algorithms [4], covariance matrix reconstruction algorithms [5–7], etc. However, the nulling formed by the above method in the interference direction is very narrow. When the interference target moves rapidly or the array platform moves rapidly, the weight vector of the beamformer cannot be updated in real time, which causes the target to move out of the narrow nulling area, after which the suppression of strong interference by the beamformer is seriously reduced.

In order to overcome the above problems, many scholars began to study the method of null broadening. References [8,9] belong to covariance matrix tapers (CMTs) in essence. Although they can effectively broaden the nulling, the virtual interference source disperses

the interference power, resulting in a shallower depth of nulling and a lower gain for the array. Reference [10] added similarity constraints on the basis of interference-plus-noise covariance matrix reconstruction, which can effectively broaden the null and ensure the width of main lobe and the height of sidelobe of the beamformer. Reference [11] applies a CMT method to broadband beamforming, which can well suppress fast interference in broadband beamforming. Reference [12] obtained the adaptive diagonal loading factor by estimating the signal-to-noise ratio in the covariance matrix of the tapered sample and combined it with the CMT method. This algorithm has good robustness and null broadening effect when there are errors in array calibration. In reference [13], an SVR-CMT algorithm was proposed that uses the CMT method to expand the null and control the sidelobe using inequality constraints and changes the optimization problem to a standard SVR problem. Reference [14] derived a new method for the reconstruction of the interference-plus-noise covariance matrix from the simplified power spectral density function. This method ensures effectiveness and has less computational complexity. Reference [15] combines CMT with a sidelobe canceller, which is more suitable for the technology in practical application, and this method also has a lower calculation cost. In reference [16], in order to reduce the computational complexity, a set of linear constraints is used to replace the quadratic constraints of the original problem. This method broadens the null and improves the array gain at the same time. The algorithm proposed in reference [17] can widen different zeros according to prior knowledge, which can save more scene degrees of freedom. In reference [18], during the reconstruction of the interference plus noise covariance matrix, the power parameter is adjusted to control the depth of the null. In addition, the signal-plus-noise covariance matrix is also reconstructed, and a new convex optimization problem is solved to obtain the desired signal guidance vector. This algorithm has certain robustness while eliminating the interference of fast motion. Reference [19] estimated the power of the interference signal through eigen subspace theory and set the virtual interference source to expand the null. This algorithm has a deeper null, lower sidelobes, and better robustness. Reference [20] combines an optimization algorithm with a general regression neural network and establishes a null model based on the data. The experiments show that this algorithm has higher operation efficiency. Reference [21] uses a numerical method to calculate the number of virtual interference sources and the reference frequency of the cone matrix, then uses the cone matrix to reconstruct the covariance matrix and finally imposes a constant beam width constraint. The method of adding virtual interference sources in this method is more complex. Reference [22] used an uncertainty set and projection technology to correct the signal steering vector and broadened null, respectively, and added diagonal loading technology to improve the robustness of the algorithm. Nevertheless, some of the above methods increase the sidelobe and main lobe width while broadening the null, which leads to a decrease in array gain.

Aiming at the above problems caused by null broadening, this paper proposes a null broadening beamforming method based on a weighted similarity vector (WSV). We attempted to use the virtual interference source to broaden the null and used the reconstructed interference-plus-noise covariance matrix to calculate the similarity vector. We constructed a weighted similar objective function, added interference-plus-noise power constraints and norm constraints to obtain low sidelobe and narrow main lobe width, and wrote the problem as a QCQP problem. Then, the semidefinite relaxation method and eigen decomposition were used to calculate the optimal solution. The simulation results show that this algorithm can maintain great gain under various error conditions and effectively suppress the sidelobe height and main lobe width. The above results show that the proposed algorithm has greater effectiveness and robustness on fast strong interference suppression.

The rest of this paper is structured as follows: Section 2 introduces the basic model of array signals and the basic theory of the Capon beamforming algorithm. Section 3 introduces the specific steps of the algorithm proposed in this paper. Section 4 shows the simulation results and analysis in various cases. Section 5 summarizes this paper.

2. Signal Model

Consider a uniform linear array (ULA) with M elements. The array element is isotropic, and the received signal is a narrowband far-field signal. Assuming that there are L incident signals, the desired signal is incident in direction θ_0, while the remaining $L-1$ interference signals are incident in direction $\theta_i (i = 1, 2, \ldots, L-1)$, respectively. The complex vector observed by the array at time t is expressed as

$$\mathbf{x}(t) = \sum_{i=0}^{L-1} \mathbf{a}_i s_i(t) + \mathbf{n}(t) \tag{1}$$

where $\mathbf{a}_i = \left[1, e^{-j\frac{2\pi d}{\lambda} sin\theta_i}, \ldots, e^{-j\frac{2\pi d}{\lambda}(M-1)sin\theta_i}\right]$ represents the steering vector of the ith signal source; $s_i(t)$ represents the waveform of the ith signal source; and $\mathbf{n}(t)$ represents additive white Gaussian noise. It is assumed that the desired signal, interference, and noise are statistically independent. The covariance matrix of the array can be expressed as

$$\boldsymbol{R_x} = E\left[\mathbf{x}(t)\mathbf{x}^H(t)\right] = \mathbf{R}_s + \mathbf{R}_{i+n} \tag{2}$$

where $E[\cdot]$ represents the statistical expected value;$(\cdot)^H$ indicates conjugate transposition. $\mathbf{R}_s = \sigma_0^2 \mathbf{a}_0 \mathbf{a}_0^H$ is the covariance matrix of the desired signal; σ_0^2 is the signal power; $\mathbf{R}_{i+n} = \sum_{i=1}^{L-1} \sigma_i^2 \mathbf{a}_i \mathbf{a}_i^H + \sigma_n^2 \mathbf{I}$ is the interference-plus-noise covariance matrix; σ_i^2 is the interference signal power; σ_n^2 is the noise power; $\mathbf{I}$ is the identity matrix.

The array output signal can be expressed as $\mathbf{y}(t) = \mathbf{w}^H \mathbf{x}(t)$, where $\mathbf{w}$ is the complex weight vector of the beamformer. Therefore, the array output SINR is defined as

$$\text{SINR} = \frac{\mathbf{w}^H \mathbf{R}_s \mathbf{w}}{\mathbf{w}^H \mathbf{R}_{i+n} \mathbf{w}} = \frac{\sigma_0^2 \left|\mathbf{w}^H \mathbf{a}_0\right|^2}{\mathbf{w}^H \mathbf{R}_{i+n} \mathbf{w}} \tag{3}$$

The Capon beamformer is realized by maximizing array output SINR:

$$\begin{cases} \underset{\mathbf{w}}{min}\, \mathbf{w}^H \mathbf{R}_{i+n} \mathbf{w} \\ s.t. \quad \mathbf{w}^H \mathbf{a}_0 = 1 \end{cases} \tag{4}$$

The solution of Formula (4) is

$$\mathbf{w}_{opt} = \frac{\mathbf{R}_{i+n}^{-1} \mathbf{a}_0}{\mathbf{a}_0^H \mathbf{R}_{i+n}^{-1} \mathbf{a}_0} \tag{5}$$

Substitute Formula (5) into Formula (3) to obtain the optimal output SINR expression

$$\text{SINR}_{opt} = \sigma_0^2 \mathbf{a}_0^H \mathbf{R}_{i+n}^{-1} \mathbf{a}_0 \tag{6}$$

In practical applications, the true value of the steering vector of the desired signal may have deviation, and the theoretical covariance matrices $\mathbf{R}_{i+n}$ and $\mathbf{R}_x$ cannot be obtained. Therefore, we usually use the sample covariance matrix $\hat{\mathbf{R}}_x$ instead of $\mathbf{R}_x$

$$\hat{\mathbf{R}}_x = \frac{1}{K} \sum_{t=1}^{K} \mathbf{x}(t)\mathbf{x}^H(t) \tag{7}$$

where K is the number of snapshots. Thus, the weight of the sample matrix inversion (SMI) algorithm is

$$\mathbf{w}_{opt} = \frac{\hat{\mathbf{R}}_x^{-1} \mathbf{a}_0}{\mathbf{a}_0^H \hat{\mathbf{R}}_x \mathbf{a}_0} \tag{8}$$

3. Proposed Algorithm

In this section, a null broadening algorithm is proposed that uses the correlation between eigenvectors and steering vectors to reconstruct the interference-plus-noise covariance matrix and incorporates weighted similarity vectors. The algorithm mainly uses the virtual interference source to broaden the null and construct a similarity vector using the reconstructed interference-plus-noise covariance matrix to constrain the main lobe width and sidelobe height of the beampattern.

3.1. Similar Vector Estimation

In order to reduce the adverse effects of widening the main lobe and increasing the sidelobe caused by broadening the null, a similar vector $\mathbf{w}_S$ is introduced. This paper uses the reconstructed interference-plus-noise covariance matrix $\hat{\mathbf{R}}_{i+n}$ and Formula (5) to calculate $\mathbf{w}_S$. In order to filter the expected signal component in the signal covariance matrix, the received signal covariance matrix $\mathbf{R}_x$ is eigendecomposed in this paper

$$\mathbf{R}_x = \mathbf{U}\boldsymbol{\Gamma}\mathbf{U}^H = \sum_{i=0}^{L-1} \gamma_i \mathbf{u}_i \mathbf{u}_i^H + \sum_{j=L}^{M-1} \gamma_i \mathbf{u}_j \mathbf{u}_j^H \tag{9}$$

where γ is the eigenvalues in descending order, $\mathbf{u}$ is the eigenvector corresponding to γ. The first L large eigenvalues are related to the received signal, and the last $M-L$ small eigenvalues are related to noise.

According to the properties of characteristic subspace

$$\boldsymbol{span}\{\boldsymbol{a_0}, \boldsymbol{a_1}, \ldots, \boldsymbol{a_{L-1}}\} = \boldsymbol{span}\{\boldsymbol{u_0}, \boldsymbol{u_1}, \ldots, \boldsymbol{u_{L-1}}\} \tag{10}$$

where $\boldsymbol{span}\{\boldsymbol{a_0}, \boldsymbol{a_1}, \ldots, \boldsymbol{a_{L-1}}\}$ is the subspace spanned by the incident signal steering vector, $span\{\mathbf{u}_0, \mathbf{u}_1, \ldots, \mathbf{u}_{L-1}\}$ is the signal subspace spanned by the eigenvector corresponding to the incident signal. Because of the linear independence between $\mathbf{u}_i (i = 0, 1, \ldots, L-1)$, the signal steering vector can be expressed linearly with $\mathbf{u}_i$

$$\mathbf{a}_i = k_{0i}\mathbf{u_0} + k_{1i}\mathbf{u}_1 + \cdots + k_{(L-1)i}\mathbf{u}_{L-1} \tag{11}$$

According to Formula (11), there is a certain linear relationship between $\mathbf{a}_i$ and $\mathbf{u}_i$; we can find the feature vector corresponding to the expected signal by calculating the correlation between the steering vector of expected signal and the feature vector

$$cor(\mathbf{a}_0, \mathbf{u}_i) = \frac{\left|{\mathbf{a}_0}^H \mathbf{u}_i\right|}{\|\mathbf{a}_0\| \|\mathbf{u}_i\|} (i = 0, 1, \ldots, L-1) \tag{12}$$

According to the maximum correlation coefficient obtained by calculating Equation (12), the corresponding eigenvector $\mathbf{u}_e$ and the corresponding eigenvalue γ_e of the desired signal can be obtained. Remove $\mathbf{u}_e$ and γ_e in Formula (9) to obtain the reconstructed interference-plus-noise covariance matrix

$$\hat{\mathbf{R}}_{i+n} = \mathbf{U}_{M\times(M-1)} \boldsymbol{\Gamma}_{M-1} \mathbf{U}^H_{M\times(M-1)} \tag{13}$$

Then, Formula (13) is substituted into Formula (5) to obtain the similarity vector $\mathbf{w}_S$

$$\mathbf{w}_s = \frac{\hat{\mathbf{R}}_{i+n}^{-1} \mathbf{a}_0}{\mathbf{a}_0^H \hat{\mathbf{R}}_{i+n}^{-1} \mathbf{a}_0} \tag{14}$$

3.2. Null Broadening

Since the incident angle $\theta_i (i = 1, 2, \ldots, L-1)$ of the interference source is known, it is only necessary to set up multiple virtual interference sources in the corner sector around θ_i to broaden the zero trap and achieve interference suppression within a certain range. In this

paper, the virtual interference interval is set as $\Delta\theta$, and the number of virtual interference sources around each interference source is N, so the widening range of each interference null is $N{\cdot}\Delta\theta$. The range of the ith corner sector is expressed as

$$\hat{\theta}_i = \left[\theta_i - \frac{N{\cdot}\Delta\theta}{2}, \theta_i + \frac{N{\cdot}\Delta\theta}{2}\right] \tag{15}$$

Next, it is necessary to determine the appropriate virtual interference source power. The Capon power spectrum expression is as follows

$$P(\theta) = \frac{1}{\mathbf{a}^H(\theta)\hat{\mathbf{R}}_x^{-1}\mathbf{a}(\theta)} \tag{16}$$

In order to ensure a better performance of interference suppression of beamformers, this paper estimates the power spectrum in the interference angle sector, finds the maximum power in the region as the power of all virtual interference sources, which can ensure the depth of the nulling while broadening the nulling. The power expression of the ith interference angle sector is

$$\hat{\sigma}_i^2 = \max\{\frac{1}{\mathbf{a}^H(\theta)\hat{\mathbf{R}}_x^{-1}\mathbf{a}(\theta)}|\theta \in \hat{\theta}_i\} \tag{17}$$

In order to estimate the noise power more accurately, this paper uses the average of the small eigenvalues of the received signal covariance matrix as the noise power

$$\hat{\sigma}_n^2 = \frac{1}{M-L}\sum_{j=L}^{M-1}\gamma_j \tag{18}$$

Then the interference-plus-noise covariance matrix can be reconstructed

$$\widetilde{\mathbf{R}}_{i+n} = \sum_{i=1}^{L-1}\hat{\sigma}_i^2\mathbf{a}(\theta)\mathbf{a}^H(\theta) + \hat{\sigma}_n^2\mathbf{I}, \quad \theta \in \hat{\theta}_i \tag{19}$$

3.3. Establishment and Solution of Objective Function

Based on the above two sections, the objective function can be established by using the obtained similarity vector and the reconstructed interference-plus-noise covariance matrix. It can be seen from the above that the calculated main lobe width and sidelobe height of the beampattern formed by similar vectors have good performance. In order to control the beampattern performance after null broadening, we use the similarity vector to construct the objective function

$$\underset{\mathbf{w}}{min}\|\boldsymbol{\lambda}(\mathbf{w} - \mathbf{w}_s)\|^2 \tag{20}$$

where $\boldsymbol{\lambda} = [\lambda_1, \lambda_2, \ldots, \lambda_M]$ represents the similar weighting value, which is set by the user according to the actual performance error of each array element. The purpose is to maintain greater similarity between elements with better performance and values in similar vectors and let elements with poor performance and more errors attempt more transformations. According to Formula (3), the smaller the denominator is, the larger the SINR will be when the expected signal is undistorted. Therefore, we constrain $\mathbf{w}^H\mathbf{R}_{i+n}\mathbf{w}$ to a small range to control the SINR lower limit of the beamformer. In order to increase the robustness of beamformer, we add norm constraints. The resulting optimization problems are as follows

$$\underset{\mathbf{w}}{min}\|\boldsymbol{\lambda}(\mathbf{w} - \mathbf{w}_s)\|^2 s.t. \quad \mathbf{w}^H\widetilde{\mathbf{R}}_{i+n}\mathbf{w} \leq \varepsilon^2\|\mathbf{w}\|^2 \leq \delta^2 \tag{21}$$

It is easy to see that problem (21) is a nonconvex quadratic constrained quadratic programming (QCQP) problem, which is usually NP-hard. Next, we mainly study how to

transform it into a convex problem and solve it. By introducing a new variable t and $t^2 = 1$, we can transform problem (21) into the following form

$$\min_{\mathbf{g}} tr\left(\mathbf{R}_0\mathbf{g}\mathbf{g}^H\right) s.t. \quad tr\left(\mathbf{R}_1\mathbf{g}\mathbf{g}^H\right) \le \varepsilon^2 tr\left(\mathbf{R}_2\mathbf{g}\mathbf{g}^H\right) \le \delta^2 tr\left(\mathbf{R}_3\mathbf{g}\mathbf{g}^H\right) = 1 \tag{22}$$

where $\mathbf{g} = \begin{bmatrix}\mathbf{w}\\ t\end{bmatrix}$, $\mathbf{R}_0 = \begin{bmatrix}\boldsymbol{\lambda}^H\boldsymbol{\lambda} & -\boldsymbol{\lambda}^H\boldsymbol{\lambda}\mathbf{w}_s\\ -\mathbf{w}_s^H\boldsymbol{\lambda}^H\boldsymbol{\lambda} & \mathbf{w}_s^H\boldsymbol{\lambda}^H\boldsymbol{\lambda}\mathbf{w}_s\end{bmatrix}$, $\mathbf{R}_1 = \begin{bmatrix}\widetilde{\mathbf{R}}_{i+n} & \mathbf{0}_{M\times 1}\\ \mathbf{0}_{1\times M} & 0\end{bmatrix}$, $\mathbf{R}_2 = \begin{bmatrix}\mathbf{I}_{M\times M} & \mathbf{0}_{M\times 1}\\ \mathbf{0}_{1\times M} & 0\end{bmatrix}$, $\mathbf{R}_3 = \begin{bmatrix}\mathbf{0}_{M\times M} & \mathbf{0}_{M\times 1}\\ \mathbf{0}_{1\times M} & 1\end{bmatrix}$. It can be seen that problems (21) and (22) have the same optimal value; the difference between the two values is only t. Then we define a semidefinite matrix $\mathbf{G} = \mathbf{g}\mathbf{g}^H$,$\mathbf{G} \succcurlyeq 0$. After the relaxation of constraint $rank(\mathbf{G}) = 1$ by the semidefinite relaxation method, then the following question forms are obtained

$$\min_{\mathbf{G}} tr(\mathbf{R}_0\mathbf{G}) s.t. \quad tr(\mathbf{R}_1\mathbf{G}) \le \varepsilon^2 tr(\mathbf{R}_2\mathbf{G}) \le \delta^2 tr(\mathbf{R}_3\mathbf{G}) = 1\mathbf{G} \succcurlyeq 0 \tag{23}$$

Problem (23) is a convex semidefinite programming (SDP) problem, which can be easily solved by using the CVX toolbox in Matlab (version: 9.4.0.813654 (R2018a)). However, the optimal solution of problem (23) is not necessarily the optimal solution of problem (22). Generally, the rank of the result obtained by problem (23) is not 1. Therefore, the first thing we should do is to judge the rank of $\mathbf{G}$. If $rank(\mathbf{G}) = 1$, the optimal solution of the original problem can be easily recovered. If $rank(\mathbf{G}) > 1$, it is necessary to obtain a suboptimal solution by solving the following problems

$$\min_{\mathbf{g}} \left\| \mathbf{G} - \mathbf{g}\mathbf{g}^H \right\|_F^2 \tag{24}$$

It is not difficult to find that the optimal solution of problem (24) is the multiplication of the maximum eigenvector of $\mathbf{G}$ and the square root of the maximum eigenvalue. Therefore, we perform EVD decomposition of $\mathbf{G}$ to obtain its maximum eigenvector $\mathbf{g}_0$ and maximum eigenvalue μ. Then the solution of problem (22) is

$$\mathbf{g}^* = \sqrt{\mu}\mathbf{g}_0 \tag{25}$$

Finally, the solution of problem (21) is obtained. Algorithm 1 summarizes the flow of the whole algorithm.

Algorithm 1: Proposed Algorithm Steps

step1:	Calculate the similarity vector using Formulas (12) and (14);
step2:	Reconstruction of interference-plus-noise covariance matrix according to Formulas (17) and (19);
step3:	Introduce a new variable t to transform problem (21) into problem (22);
step4:	Construct semidefinite matrix $\mathbf{G} = \mathbf{g}\mathbf{g}^H$ to transform problem (22) into standard SDP problem;
step5:	Judge the rank of $\mathbf{G}$, If $rank(\mathbf{G}) = 1$, calculate $\mathbf{g}^*$ according to $\mathbf{G} = \mathbf{g}^*\mathbf{g}^{*H}$; Otherwise, skip to step 6;
step6:	Calculate $\mathbf{g}^*$ using Formula (25);
step7:	Calculate $\mathbf{w}^*$.

4. Simulation Analysis

The simulation in this paper is based on a linear sonar array with 32 elements and half wavelength element spacing. The desired signal incidence direction is set as 0°, the two interference signal incidence directions are set as -20° and 40°, and the interference-to-noise ratios (INRs) are set as 15 dB and 20 dB, respectively. The sound speed is set to $c = 1500\,\mathrm{m/s}$. The noise is set to obey the Gaussian distribution of $N(0, 1)$. All experimental results are the results of 100 Monte Carlo tests.

4.1. Performance Comparison between the Proposed Algorithm and Other Algorithms

In this section, the proposed algorithm (WSV) is compared with the sample matrix inversion (SMI) algorithm, the covariance matrix tapers (CMT) algorithm, the linear constraint sector suppressed (LCSS) algorithm, Yu's beamformer [19], and the theoretical optimal value algorithm. The broadening ranges of zero depression are both [−23°,−17°] and [37°,43°]. The virtual interference interval is 0.1°. The noise figure of the algorithm in reference [19] is set to 0.1. The parameters of the algorithm proposed in this paper are as follows: $\varepsilon = 0.01$, $\delta = 1/M$, $\boldsymbol{\lambda} = [diag(0.5 \cdot \mathbf{I}_{\frac{M}{2} \times \frac{M}{2}}), diag(0.8 \cdot \mathbf{I}_{\frac{M}{2} \times \frac{M}{2}})]$.

4.1.1. Beampattern Effect in Ideal State

The simulation parameters were set as follows: the number of snapshots is 600, and the desired signal-to-noise ratio (SNR) is 0 dB. It can be seen from Figure 1 that the main lobe directions of the five algorithms are aligned to 0°, and null is formed in the directions of −20° and 40°. However, SMI, CMT, and LCSS have high sidelobes and poor noise suppression, and the nulling depth is relatively shallow. Both the algorithm proposed in reference [19] and WSV have low sidelobes and deep null, indicating that the two algorithms have a good interference suppression effect and can effectively suppress interference within the range.

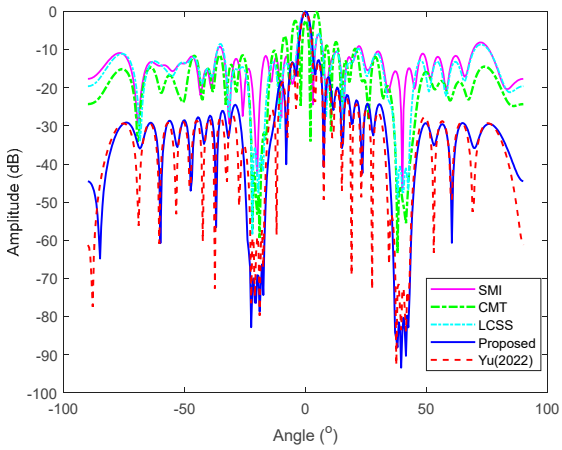

Figure 1. Beampatterns of different algorithms in ideal state [19].

4.1.2. Output SINR Performance in Ideal State

The simulation parameters in Figure 2 are set as follows: the number of snapshots is 600 and the input SNR range is [−20,30] dB. It can be seen from Figure 2 that the output SINR of SMI and LCSS algorithms increases with the increase in input SNR at a low signal-to-noise ratio, and the increase tends to be gradual after SNR = 0. The SINR of CMT also shows an upward trend in general and a downward trend in the end. This is because the above three algorithms do not remove the desired signal component in the received signal when calculating the weight vector, resulting in the signal component being suppressed as interference under the condition of a large signal-to-noise ratio. Compared with the algorithm in reference [19], WSV has a better effect in each SNR case, a stable growth trend, and always approximates the theoretical optimal value. The simulation parameters in Figure 3 are set as follows: the input SNR is 0 dB and the snapshot number range is [40,400]. It is easy to see that the output SINR of SMI, CMT and LCSS are low under the condition of low snapshot number. With the increase in snapshot number, the output SINR gradually increases and tends to be flat. The algorithm in reference [19] and WSV show a horizontal trend as a whole, which can still maintain good performance under low snapshot conditions, and the WSV is slightly better than that in reference [19], which is closer to the theoretical optimal value.

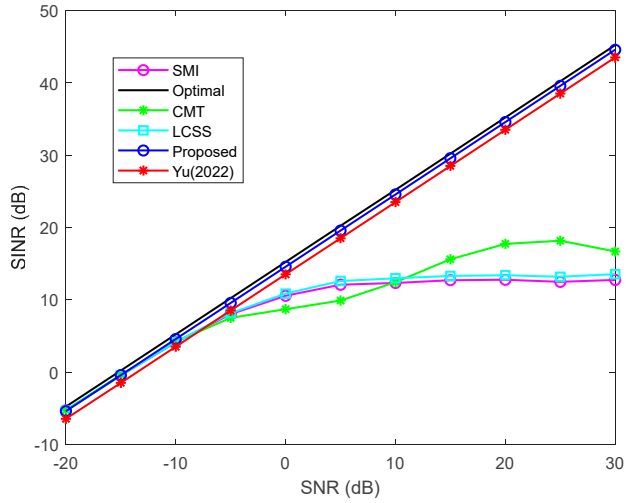

Figure 2. Output SINR under different input SNRs in ideal state [19].

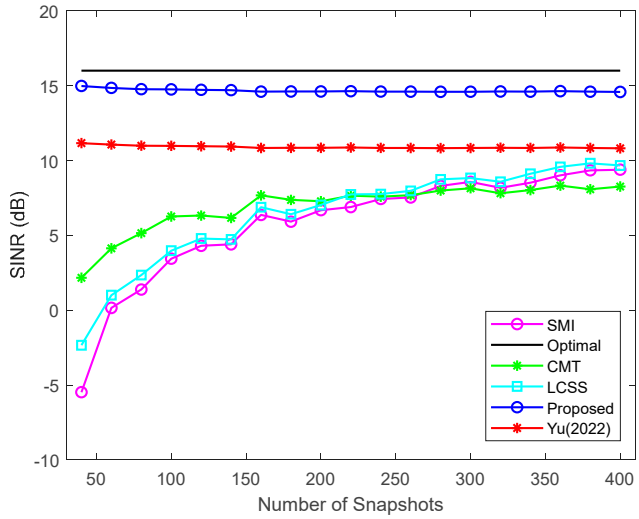

Figure 3. Output SINR under different snapshot numbers in ideal state [19].

4.1.3. Output SINR Performance under Amplitude and Phase Disturbance Errors

The parameters set in Sections 4.1.2 and 4.1.3 are basically the same. On this basis, we add amplitude and phase disturbance errors. It is assumed that the amplitude error of each sensor follows $N(1, 0.1^2)$ and the phase error follows $N\left(0, 20^{\circ 2}\right)$. The m-th element of the steering vector after adding amplitude and phase errors is expressed as

$$\mathbf{a}(\theta)_m = (1 + A_m)e^{-j(\frac{2\pi md}{\lambda} sin\theta + \epsilon_m)} \tag{26}$$

where A_m represents amplitude error and ϵ_m represents phase error.

Figure 4 shows that the performances of SMI, CMT, and LCSS drop sharply due to the addition of amplitude and phase errors, which shows that their robustness is poor. The upward trend of the algorithm in reference [19] is stable. Compared with the algorithm in reference [19], WSV has better performance and is closer to the theoretical optimal value while ensuring the growth trend. It can be seen that the algorithm proposed in reference [19] and this paper have good robustness. The results shown in Figure 5 are almost identical to those in Figure 3. The difference is that SMI, CMT, and LCSS only show a small increase trend before the number of snapshots is 100, and then they keep floating up and down and are affected by amplitude and phase errors. All values are low and the performance is poor. Reference [19] and WSV have strong robustness, and the performance is almost unaffected

by the number of snapshots. Although the addition of amplitude and phase errors can affect the steering vector **a**, according to Equation (8), it can be seen that the final impact of this error is still the weighted vector **w.** Meanwhile, the algorithm proposed in this article directly optimizes **w**, thus effectively reducing the impact of this error.

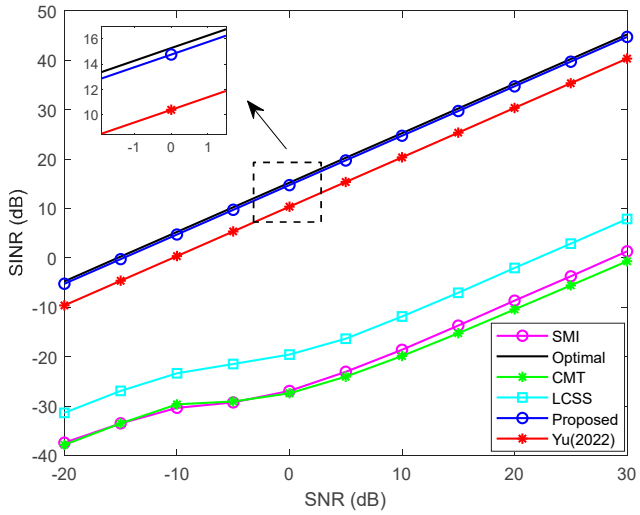

Figure 4. Output SINR under different input SNRs with amplitude and phase perturbation errors [19].

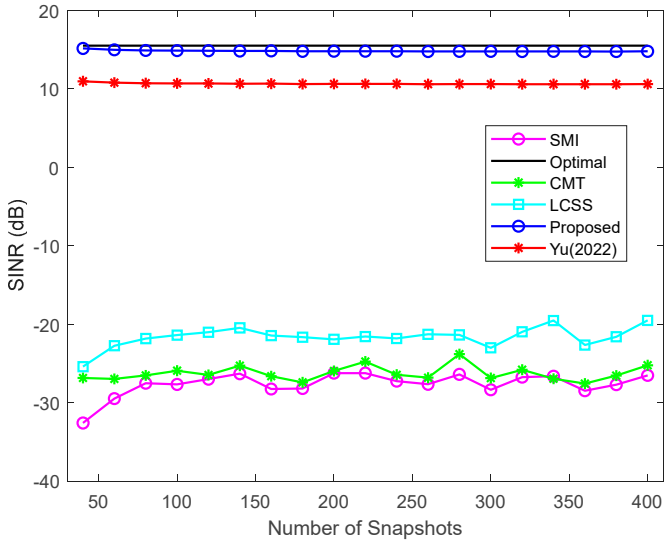

Figure 5. Output SINR under different snapshot numbers with amplitude and phase perturbation errors [19].

4.1.4. Output SINR Performance with Array Element Position Error

The parameters of Section 4.1.4 are the same as those of Section 4.1.2. Considering the disturbance of waves in the underwater environment, we add the position error of the array element in this simulation to test the robustness of the beamformer. Assuming that the position error $\Delta d_i (i = 1, 2, \ldots, M)$ of each array element is uniformly distributed between $[-0.1\lambda, 0.1\lambda]$, the actual signal steering vector becomes

$$\bar{\mathbf{a}}(\theta) = \boldsymbol{\psi}\mathbf{a}(\theta) = diag(e^{-j\frac{2\pi\Delta d_1}{\lambda}sin\theta}, e^{-j\frac{2\pi\Delta d_2}{\lambda}sin\theta}, \ldots, e^{-j\frac{2\pi\Delta d_M}{\lambda}sin\theta}) \quad (27)$$

The results in Figure 6 show that the performance of SMI, CMT, and LCSS are seriously degraded, and the SINR are almost unchanged after slowly rising under low signal-to-noise ratio conditions. The robustness of WSV is consistent with that in reference [19], but the

output SINR is about 4 dB higher than the algorithm in reference [19] under various signal-to-noise ratio conditions. Figure 7 still shows the superior robustness of the algorithm in the reference [19] and WSV, and the good performance not affected by the number of snapshots in the environment where the array element position produces errors.

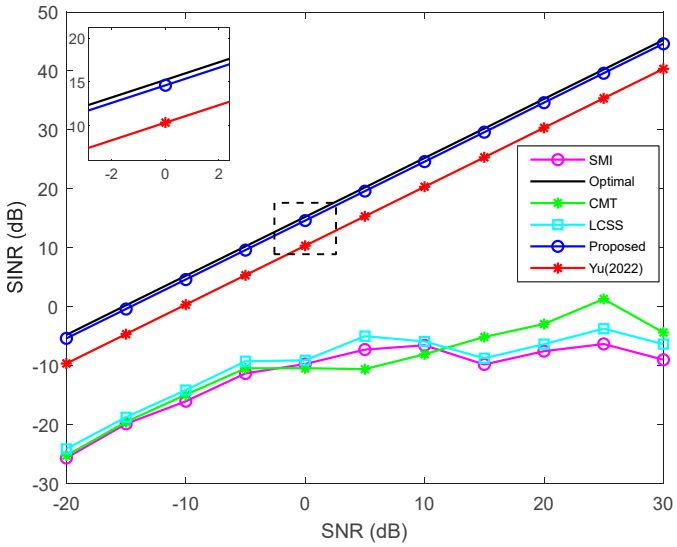

Figure 6. Output SINR under different input SNRs with array element position error [19].

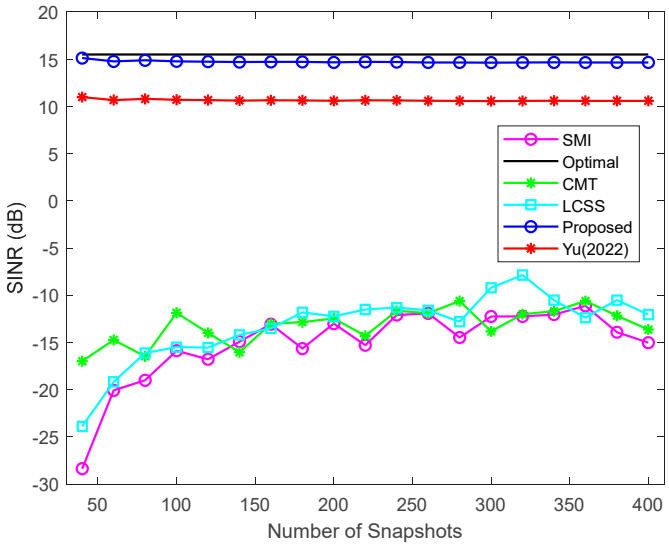

Figure 7. Output SINR under different snapshot numbers with array element position error [19].

4.2. Effect of Different Parameters on the Performance of the Proposed Algorithm

In this section, we focus on the performance of the proposed algorithm under different parameter conditions. The following simulation parameters are set as SNR = 0 dB, the number of snapshots is 600, and other parameters are consistent with Section 4.1.

4.2.1. Effect of Parameter ε on Beamformer Performance

Section 4.2.1 studies the performance differences of a beamformer under different ε conditions, in which the null width is 6°. It can be clearly seen from Figure 8 that with the decrease in ε, the null of the beamformer gradually becomes deeper, and the ability to suppress interference becomes stronger. This is because the reduction in ε restricts the interference-plus-noise power to a smaller range. The closer ε is to 0, the better interference will be suppressed. Figure 9 shows that the smaller the value of ε, the larger the output

SINR under the same SNR. This is because the denominator of the SINR expression is constrained to a smaller range, so the output SINR is larger.

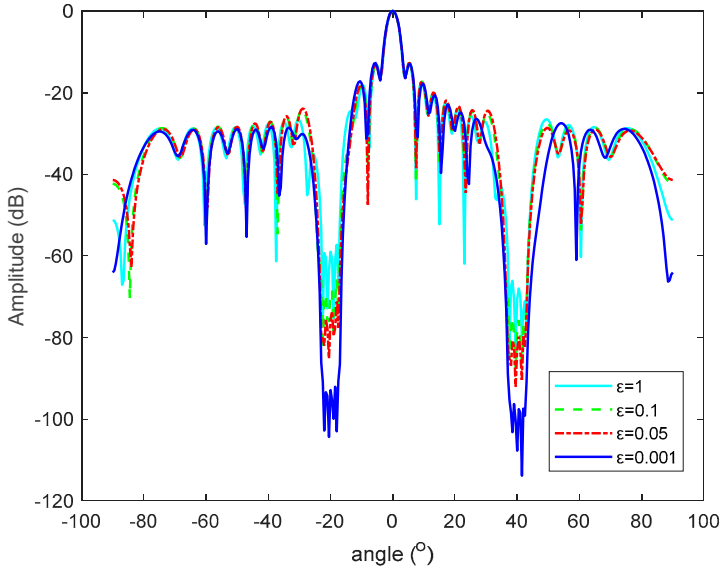

Figure 8. Beampattern under different ε conditions.

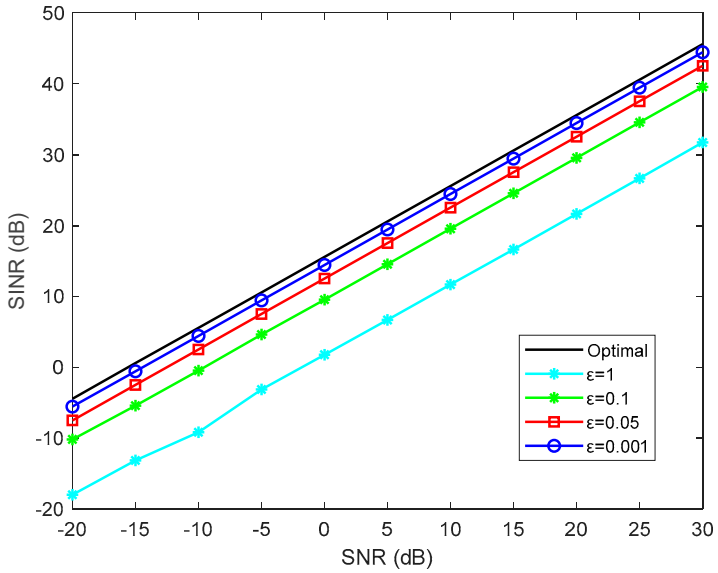

Figure 9. Output SINR under different ε conditions.

4.2.2. Effect of Nulling Width on Beamformer Performance

Section 4.2.2 sets ε to 0.01 and studies the performance of beamformer under different null width. It can be seen from Figure 10 that with the increase in the null width, the null depth does not decrease significantly. This is because the power of the virtual interference source used in this paper is the maximum power in the broadened area, so the interference power will not decrease with the change in the null width. It can be seen from Figure 11 that the change in the null width has little effect on the output SINR. When the null width is 4° and 16°, the output SINR only has a 1 dB difference. The simulation shows that the performance of the proposed algorithm is not sensitive to the change in the null width and has an obvious effect on suppressing the strong interference of fast movement, with strong robustness.

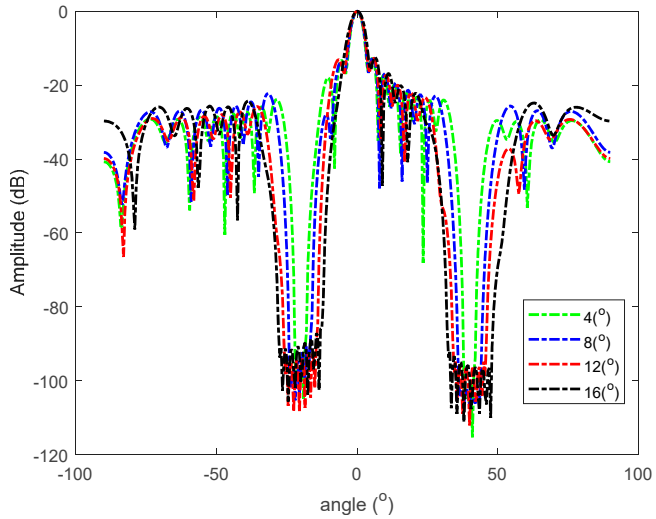

Figure 10. Beampatterns with different nulling widths.

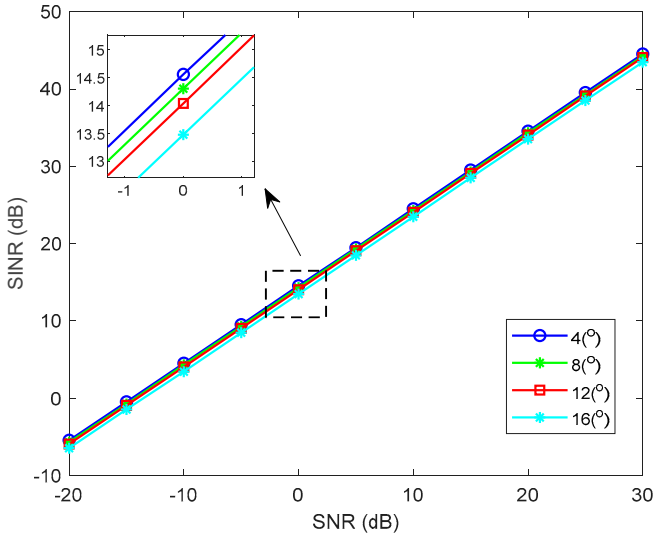

Figure 11. Output SINR with different null width.

5. Conclusions

In this paper, a new null broadening Capon beamformer is proposed to effectively suppress the influence of strong interference caused by rapid underwater movement. The algorithm uses the covariance matrix after removing the desired signal components to calculate the similarity vector. Then the null trap is broadened by setting virtual interference sources around the interference. Next, the difference between the weight vector to be calculated and the similar vector is minimized, and interference and noise power constraints are added. Finally, we use the semidefinite relaxation technique and eigen decomposition to calculate the optimal solution. The simulation results show that the algorithm can effectively suppress the sidelobe height while ensuring the deep null, and the null depth will not become shallow with the increase in the null width. Application in different scenes reflects the effectiveness and robustness of the beamformer.

Author Contributions: Conceptualization, software, writing—original draft, Y.W.; methodology, formal analysis, writing—review and editing, Z.Z. All authors have read and agreed to the published version of the manuscript.

Funding: This work was funded by the Graduate Research and Innovation Projects of Jiangsu Province (KYCX23_3907) and National Natural Science Foundation of China (61871203).

Institutional Review Board Statement: Not applicable.

Informed Consent Statement: Not applicable.

Data Availability Statement: The data that support the findings of this study are available from the corresponding author upon reasonable request.

Acknowledgments: The authors would like to express their deep appreciation to the reviewers who provided very useful criticism and many insightful remarks.

Conflicts of Interest: The authors declare no conflict of interest.

References

1. Capon, J. High-resolution frequency-wavenumber spectrum analysis. *Proc. IEEE* **1969**, *57*, 1408–1418. [CrossRef]
2. Li, Y.; Ma, H.; Yu, D.; Cheng, L. Iterative robust Capon beamforming. *Signal Process.* **2016**, *118*, 211–220. [CrossRef]
3. Zhang, M.; Zhang, A.; Yang, Q. Robust adaptive beamforming based on conjugate gradient algorithms. *IEEE Trans. Signal Process.* **2016**, *64*, 6046–6057. [CrossRef]
4. Tian, Z.; Bell, K.L.; Van Trees, H.L. A recursive least squares implementation for LCMP beamforming under quadratic constraint. *IEEE Trans. Signal Process.* **2001**, *49*, 1138–1145. [CrossRef]
5. Huang, J.; Su, H.; Yang, Y. Robust adaptive beamforming for MIMO radar in the presence of covariance matrix estimation error and desired signal steering vector mismatch. *IET Radar Sonar Navig.* **2020**, *14*, 118–126. [CrossRef]
6. Xie, Z.; Fan, C.; Zhu, J.; Huang, X. Robust beamforming for wideband array based on spectrum subspaces. *IET Radar Sonar Navig.* **2020**, *14*, 1319–1327. [CrossRef]
7. Liu, J.; Xie, W.; Gui, G.; Zhang, Q.; Zou, Y.; Wan, Q. Adaptive beamforming algorithms with robustness against steering vector mismatch of signals. *IET Radar Sonar Navig.* **2017**, *11*, 1831–1838. [CrossRef]
8. Zatman, M.; Guerci, J.R. Comments on "Theory and application of covariance matrix tapers for robust adaptive beamforming" [with reply]. *IEEE Trans. Signal Process.* **2000**, *48*, 1796–1800. [CrossRef]
9. Ma, Y.; Lu, D.; Wang, W.; Wang, L.; Wu, R. A high-dynamic null-widen GPS anti-jamming algorithm based on statistical model of the changing interference DOA. In Proceedings of the China Satellite Navigation Conference (CSNC) 2014, Nanjing, China, 21–23 May 2014; Springer: Berlin/Heidelberg, Germany, 2014; Volume I.
10. Qian, J.; He, Z.; Xie, J.; Zhang, Y. Null broadening adaptive beamforming based on covariance matrix reconstruction and similarity constraint. *EURASIP J. Adv. Signal Process.* **2017**, *1*, 1. [CrossRef]
11. Yang, X.; Li, S.; Long, T.; Sarkar, T.K. Adaptive null broadening method in wideband beamforming for rapidly moving interference suppression. *Electron. Lett.* **2018**, *54*, 1003–1005. [CrossRef]
12. Li, W.; Zhao, Y.; Ye, Q.; Yang, B. Adaptive antenna null broadening beamforming against array calibration error based on adaptive variable diagonal loading. *Int. J. Antennas Propag.* **2017**, *2017*, 3265236. [CrossRef]
13. Liu, F.; Wu, Y.; Duan, H.; Du, R. SVR-CMT algorithm for null broadening and sidelobe control. *Prog. Electromagn. Res.* **2018**, *163*, 39–50. [CrossRef]
14. Mohammadzadeh, S.; Kukrer, O. Robust adaptive beamforming for fast moving interference based on the covariance matrix reconstruction. *IET Signal Process.* **2019**, *13*, 486–493. [CrossRef]
15. Liu, Z.; Zhao, S.; Zhang, G.; Jiao, B. Robust adaptive beamforming for sidelobe canceller with null widening. *IEEE Sens. J.* **2019**, *19*, 11213–11220. [CrossRef]
16. Amar, A.; Doron, M.A. A linearly constrained minimum variance beamformer with a pre-specified suppression level over a pre-defined broad null sector. *Signal Process.* **2015**, *109*, 165–171. [CrossRef]
17. Liu, Z.; Zhao, S.; Zhang, G. Flexible robust adaptive beamforming method with multiple separately widened nulls. *Electron. Lett.* **2020**, *56*, 957–959. [CrossRef]
18. Yang, J.; Lu, J.; Liu, X.; Liao, G. Robust null broadening beamforming based on covariance matrix reconstruction via virtual interference sources. *Sensors* **2020**, *20*, 1865. [CrossRef]
19. Yu, Z.; Cui, W.; Du, Y.; Ba, B.; Quan, M. Null Broadening Robust Adaptive Beamforming Algorithm Based on Power Estimation. *Sensors* **2022**, *22*, 6984. [CrossRef]
20. Xiao, X.; Lu, Y. Data-based model for wide nulling problem in adaptive digital beamforming antenna array. *IEEE Antennas Wirel. Propag.* **2019**, *18*, 2249–2253. [CrossRef]
21. Yang, X.; Li, S.; Sun, Y.; Long, T.; Sarkar, T.K. Robust wideband adaptive beamforming with null broadening and constant beamwidth. *IEEE Trans Antennas Propag.* **2019**, *67*, 5380–5389. [CrossRef]
22. Yang, B.; Li, W.; Li, Y.; Zhang, Q. Robust adaptive null broadening beamforming based on subspace projection. *Int. J. Electron.* **2023**, *110*, 184–198. [CrossRef]